


Interfacial reaction and mechanical properties for Cu/Sn/Ag system low temperature transient liquid phase bonding

Huakai Shao^{1,2,3}  · Aiping Wu^{1,2,3} · Yudian Bao^{1,2,3} · Yue Zhao^{1,2,3} · Guisheng Zou^{1,2,3}

Received: 26 November 2015 / Accepted: 17 January 2016 / Published online: 27 January 2016
© The Author(s) 2016. This article is published with open access at Springerlink.com

Abstract Low temperature transient liquid phase (LTTLTP) bonding is a promising technology to enable in high temperature electronic packaging. In this study, interfacial reaction and mechanical characterizations for Cu/Sn/Ag system LTTLTP bonding at temperatures ranging from 260 to 340 °C for various time were investigated. Experimental results showed that Cu and Ag substrate independently reacted with molten Sn, and the growth of IMCs on one side was hindered by the opposite IMCs layer after scalloped Cu₆Sn₅ contacted with the Ag₃Sn, and there was no ternary alloy phase formed all the time. Pores were found and distributed at the Cu₆Sn₅/Ag₃Sn interface or between grain boundaries after the residual Sn was fully consumed, however, they gradually disappeared with continuing reaction of that Cu₆Sn₅ phase converted into Cu₃Sn phase. Shear strength of the LTTLTP joints increased with increasing bonding time, and the adhesive strength of Cu₆Sn₅/Ag₃Sn interface was weaker than that of the Cu₃Sn/Ag₃Sn interface. The rupture behaviors were also discussed with a fracture model. As follow, cracks initiated in the pore and mainly propagated along the Cu₆Sn₅/Ag₃Sn interface for the joint consisted of layered Cu₃Sn, Cu₆Sn₅ and Ag₃Sn IMCs, however, failure path only passed through the Cu₃Sn layer after Cu₆Sn₅ islands were completely transformed.

1 Introduction

With development of the electronic materials and demand for industries such as automotive, aerospace and deep-well drilling, many power devices have to be operated in harsh environment, which needs the corresponding assemblies have excellent thermal reliability even exceeding 300 °C [1–3]. For example, problems appear when traditional silicon (Si) power devices are operated at temperatures above 200 °C, as self-heating at higher power levels results in high internal junction temperatures and leakages; however, some new type wide band-gap semiconductors have much higher maximum operating temperature, for example, silicon carbide (SiC) devices have been demonstrated at 600 °C [1, 4]. It is a challenge for academia and industrial circles to explore appropriate interconnection technology to accommodate this trend. Nowadays, high temperature packaging techniques, including Cu–Cu thermo-compression bonding [5], soldering with high-temperature solders like Au–Sn alloy [6], nano-silver particle sintering [7] and low temperature transient liquid phase (LTTLTP) bonding, are all commonly recognized as potential candidates. However, LTTLTP bonding, also called solid–liquid interdiffusion (SLID) bonding [8] and diffusion soldering [9], has been proven to be a promising approach in application to power devices. It is first investigated by Bernstein [10] in 1966, low melting point metal or alloy (i.e. Sn, In–Sn) as interlayer and high melting point metal (i.e. Cu, Ag) as substrate are used in this method, and the bonded joint is entirely composed of intermetallic compounds (IMCs), which have higher re-melting temperature compared with bonding condition and withstand operation in excess of 400 °C.

In LTTLTP studying, many systems have been developed for the past decades. For the base metal, it is majorly

✉ Huakai Shao
shk13@mails.tsinghua.edu.cn

¹ Department of Mechanical Engineering, Tsinghua University, Beijing 100084, China

² State Key Laboratory of Tribology, Tsinghua University, Beijing 100084, China

³ Key Laboratory for Advanced Materials Processing Technology, Ministry of Education, Tsinghua University, Beijing 100084, China

focused on the Cu, Ag and Au series [9, 11–19], while researches on Ni, Pd and Pt have been also reported in recent years [20, 21]. The primary criterion for selection of an interlayer is melting point and compatibility with base metal such as high solubility and high diffusivity. Wherein, unitary system contains Sn (232 °C) and In (156 °C), and binary or ternary system includes In–Sn (120 °C), In–Bi (89 °C), Sn–Bi (139 °C) and In–Sn–Bi (60 °C) alloys [22]. In general, LTTLP bonding process is often conducted at temperatures higher than melting point of the interlayer by a range of 15–120 °C, and bonding time mainly depends on the thickness of the interlayer [9, 15–19]. Most of studies concentrated on microstructure evolution [9, 21, 23], interfacial reaction [12, 13, 21], kinetics of the IMCs growth [12, 13], thermal reliability [24, 25], and electrical or mechanical behaviors of the joints [9, 11, 23] for above systems applied in electronic packaging and interconnects.

As electronic materials that are widely utilized in packaging, both copper and silver have excellent physical, electrical and mechanical properties, such as good thermal conductivity, good electrical conductivity and good ductility. However, mechanisms about the Cu/Sn/Ag system LTTLP bonding, like interfacial reaction, mechanical properties, even feasibility, have not been reported so far. No information is available on the phase transformation, evolution of the IMCs and mechanical behaviors for the joint. Therefore, it is significantly worth knowing more about Cu/Sn/Ag isothermal bonding at low temperature. In the present work, interfacial reaction of Cu/Sn/Ag LTTLP bonding at temperatures ranging from 260 to 340 °C, especially for the combination of Cu–Sn IMCs and Ag–Sn IMCs, was systematically investigated, in addition, mechanical characterizations of the joints were also discussed.

2 Experimental procedure

In this work, polished pure Cu rod with dimension of Φ 10 mm \times 5.5 mm and Φ 6 mm \times 5.5 mm sized pure Cu rod plated with 35 μ m thick Ag layer, were used as substrates to simulate the Cu/Ag system. A commercially available 20 μ m thick pure Sn foil (99.9 %) with 6 mm in diameter was used as interlayer. The sequential cleaning process with dilute nitric acid, deionized water and anhydrous ethanol was applied on the substrate to remove the oxides and impurities from the surface, and Sn foil was also cleaned in acetone. After alignment, as depicted in Fig. 1, the Cu/Sn/Ag sandwich structure was placed into a vacuum furnace and loaded by a stainless steel bulk with weight of 283 g (about 0.1 MPa). Heating process was carried out when the vacuum degree was lower than 2×10^{-3} Pa, and

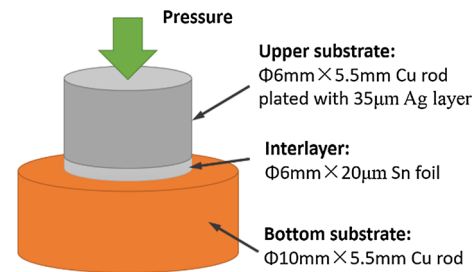


Fig. 1 Schematic diagram of the assembly structure for bonding process

the samples were isothermally bonded at 260, 300 and 340 °C for 15–420 min, respectively.

The bonded samples for microstructure analysis were mounted and polished to prepare metallographic examinations, and then they were observed using scanning electron microscope (SEM). Electro-probe micro-analyzer (EPMA) analysis was also adopted to evaluate the distribution of Cu, Sn and Ag atoms on the cross-section. In addition, the joints bonded at 300 °C for different time were executed with shearing test, which was conducted on the Gleeble-1500D thermal simulated test machine and the shear rate was 1 mm/min. The shear strength can be calculated by:

$$\tau = \frac{F}{A} \quad (1)$$

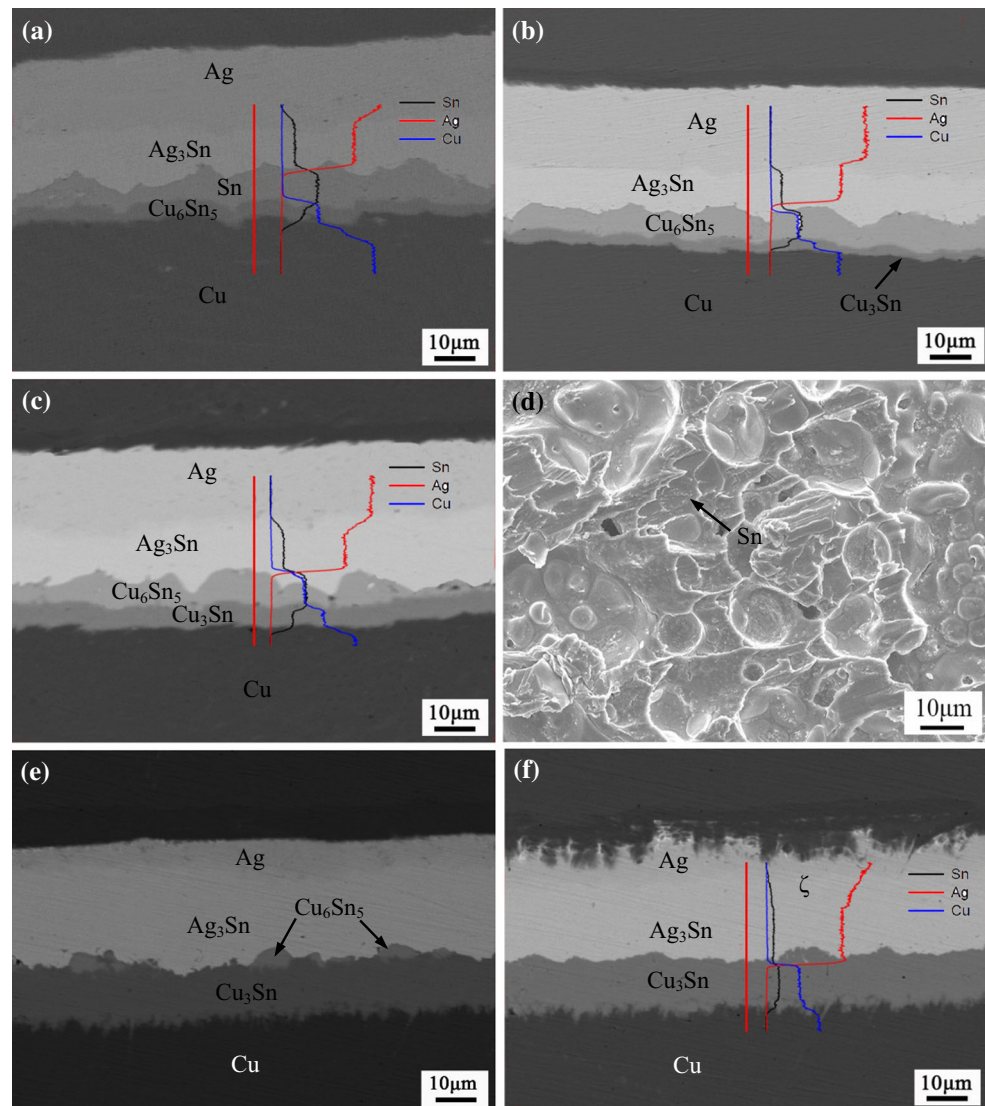
where F is the peak value of force-stroke curve, and A is the area of Φ 6 mm electroplated-silver Cu substrate. Three values under one condition was averaged in this study. At last, fracture surfaces for some typical joints were examined with SEM, and energy disperse spectroscopy (EDS) was also used to identify compositions of the indicated zones.

3 Results and discussion

3.1 Interfacial microstructure

After bonding at 300 °C for various time, cross-sections of the joints were evaluated with SEM and EPMA. Figure 2 showed the evolution process of the interfacial microstructure between Cu and Ag substrate. For 15 min (Fig. 2a), molten Sn reacted with the components that diffused from substrates but still remained as a layered structure after isothermal solidification, and thin layers of scalloped Cu_6Sn_5 and Ag_3Sn were found on the surface of Cu and Ag substrate, respectively. Furthermore, the thickness of Ag_3Sn layer was larger than that of Cu_6Sn_5 layer, which indicated that Ag/Sn reaction was faster than

Fig. 2 Cross-sectional microstructure of the joints bonded at 300 °C for **a** 15 min, **b** 60 min, **c** 150 min, **e** 300 min and **f** 420 min in backscattered electron mode; and **d** fracture surface for 60 min



Cu/Sn reaction during solid–liquid interdiffusion. The EPMA line-scanning results for the distribution of Cu, Sn and Ag atoms were consistent with the transverse microstructure of the joint, and there was no intersection occurred at the position of Sn layer for the Cu and Ag diffusion curves, which revealed that no ternary alloy phase was formed at this time.

In the joint bonded for 60 min (Fig. 2b), Sn could not be clearly observed in this SEM objective area; however, some tearing-like zones were noticed on the fracture surface of the joint that demonstrated an ultra-thin residual Sn layer still existed (Fig. 2d). This phenomenon also implied heterogeneous growth of the Ag_3Sn or Cu_6Sn_5 grains in different areas, owing to anisotropic mass flow. In addition, it was found that a thin Cu_3Sn layer appeared between Cu_6Sn_5 layer and Cu substrate at this moment, which had columnar crystal morphology that was different with the

scalloped Cu_6Sn_5 grain [8, 13]. EPMA elemental distribution curves were also in agreement with the interfacial microstructure, and Cu distribution curve did not intersect with that of Ag as well.

As the bonding time prolonged to 150 min (Fig. 2c), residual Sn was completely consumed and the Cu_6Sn_5 layer contacted with Ag_3Sn layer, and the thickness of the Cu_3Sn layer increased with increasing dwell time. Moreover, EPMA measurements for elemental diffusion were also similar to the interfacial microstructure, and the Cu and Ag scanning curves did not intersect with each other.

Several island-like Cu_6Sn_5 IMCs were isolated into separate areas after bonding for 300 min (Fig. 2e), since unstable Cu_6Sn_5 phase continually converted into Cu_3Sn phase, and the scalloped Ag_3Sn also began to contact with Cu_3Sn layer. Furthermore, it could be found that the $\text{Cu}_3\text{Sn}/\text{Ag}_3\text{Sn}$ interface was more planar in comparison to the

$\text{Cu}_6\text{Sn}_5/\text{Ag}_3\text{Sn}$ interface, and the scalloped Ag_3Sn grains seemed to evolve into plane shape to combine with columnar Cu_3Sn grains. This revealed that diffusion processes probably took place on the two sides of the Cu–Sn IMCs/ Ag –Sn IMCs (i.e. $\text{Cu}_6\text{Sn}_5/\text{Ag}_3\text{Sn}$) interface, respectively, and changed the interfacial morphology.

When the bonding time reached to 420 min (Fig. 2f), it was finished that the dispersive Cu_6Sn_5 compounds transformed into Cu_3Sn compounds on the Cu side, meanwhile, ζ phase layer probably was formed between Ag substrate and Ag_3Sn layer according to the Ag and Sn EPMA distribution curves, which presented a long-distanced transition characterization where closed to the Ag/ Ag_3Sn interface and differed from the previous measurements. It was because that the content of Sn in ζ phase have an extensive range of 12.8–25.4 at.% according to binary Ag–Sn phase diagram [22].

Interestingly, it could be noticed that there was no intersection for Cu and Ag EPMA scanning curves at the $\text{Cu}_6\text{Sn}_5/\text{Ag}_3\text{Sn}$ or $\text{Cu}_3\text{Sn}/\text{Ag}_3\text{Sn}$ interface all the way, so we deduced that no ternary alloy phase was formed in Cu/Sn/Ag system LTTLT joints. On the other hand, area distributions of Cu, Sn and Ag atoms for the joint bonded after 420 min were evaluated by EPMA method, as shown in Fig. 3, Cu atoms did not be detected on the Ag_3Sn side (Fig. 3b) and no Ag atoms were examined on the Cu_3Sn side (Fig. 3d), and their mapping images sketched a similar boundaries with the SEM images (Fig. 3a) at the $\text{Ag}_3\text{Sn}/\text{Cu}_3\text{Sn}$ interface. These detection data also demonstrated the above deduction to some extent. In addition, it could be distinctly seen that about 7 μm -thick light transitional band appeared in the area distribution graph of Sn atoms (Fig. 3c), which exactly corresponded to the layer of ζ phase.

LTTLT bonding for Cu/Sn/Ag system was also performed at 260 and 340 °C to further explore the interfacial reaction, especially for the combination process of Cu–Sn IMCs and Ag–Sn IMCs. Before experimental observation, metallographic samples with residual Sn were mildly etched by corrosion solution, as shown in Figs. 4 and 5, and the IMCs morphology was obtained from SEM. As similar with the joints bonded at 300 °C, scalloped Cu_6Sn_5 and Ag_3Sn grains were formed on the surface of the Cu and Ag substrate, respectively, and size of Ag_3Sn grain was notably larger than that of Cu_6Sn_5 grain, which also indicated that growth rate of Ag_3Sn was more rapid than the Cu_6Sn_5 . With increasing temperature and dwell time, the thickness of both Cu_6Sn_5 and Ag_3Sn layer increased until the residual Sn was completely consumed. As Cu_6Sn_5 layer initially contacted with Ag_3Sn layer, the IMCs on one side became a barrier for the growth of the IMCs on the other side (Figs. 4b, 5b), since Cu and Ag atoms could not interdiffuse into another IMCs side. In addition, a few small-

sized pores were observed at the interface (Fig. 4b), and the residual Sn was isolated into island-like areas depicted in Figs. 4b and 5b. Pores still existed when Sn was entirely disappeared, as shown in Fig. 4c. However, these pores were never found with continuing reaction and the Cu–Sn IMCs combined well with the Ag–Sn IMCs (Fig. 4d). According to reaction behaviors of the Cu–Sn–Ag LTTLT bonding as analyzed above, it was supposed that disappearance of the pores with longer bonding time was controlled by the self-diffusion processes on the two sides of the Cu–Sn IMCs/ Ag –Sn IMCs interface. Interestingly, it could be noticed that Cu_3Sn layer grew very slowly at 260 °C in comparison of Fig. 4c, d, and no significant thickening was observed with the prolonging dwell time; furthermore, the interface of Cu–Sn IMCs and Ag–Sn IMCs still maintained remarkable waved-shape though bonding process performed for a long time. This phenomenon was very different from the conditions higher than 300 °C (Figs. 2, 5), which resulted from the lower diffusion rate of Cu and Ag atoms under solid state at lower temperature.

According to binary Cu–Sn and Ag–Sn phase diagrams [22], Cu_6Sn_5 and Ag_3Sn phase have high remelting temperature of 415 and 480 °C, respectively, and that of the Cu_3Sn and ζ phase even exceed 600 °C. Therefore, Cu/Sn/Ag LTTLT joints have excellent thermal reliability. Furthermore, the Cu–Sn IMCs and Ag–Sn IMCs combine with each other very well after bonding for a long time (i.e. 300 °C for 420 min) according to the interfacial microstructure. In conclusion, it can be considered that Cu/Sn/Ag LTTLT bonding is a potential system that is used in high temperature packaging applications.

3.2 Mechanical characterizations

With change of the microstructure of the LTTLT joints, mechanical behaviors varied accordingly during shear tests. As shown in Fig. 6, shear strength of the joint bonded at 300 °C increased with bonding time from 23.4 MPa for 15 min to 60.2 MPa for 420 min. It could be seen that the shear strength dramatically increased from 15 to 30 min with the reduction of the layered Sn, but slowly increased after bonding time reached to 60 min though island-like Sn existed in the joint. After the IMCs layers on two different sides contacted with each other, shear strength increased slowly with the bonding time, due to phase transformation and disappearance of pores under solid-state reaction.

Fractures of several typical LTTLT joints were observed using SEM to discuss their rupture behaviors. Figure 7 showed the fracture surface of the joint produced at 300 °C for 150 min, in which the residual Sn was totally consumed and the Cu_6Sn_5 layer contacted with Ag_3Sn layer as mentioned above. Both intergranular fracture planes and

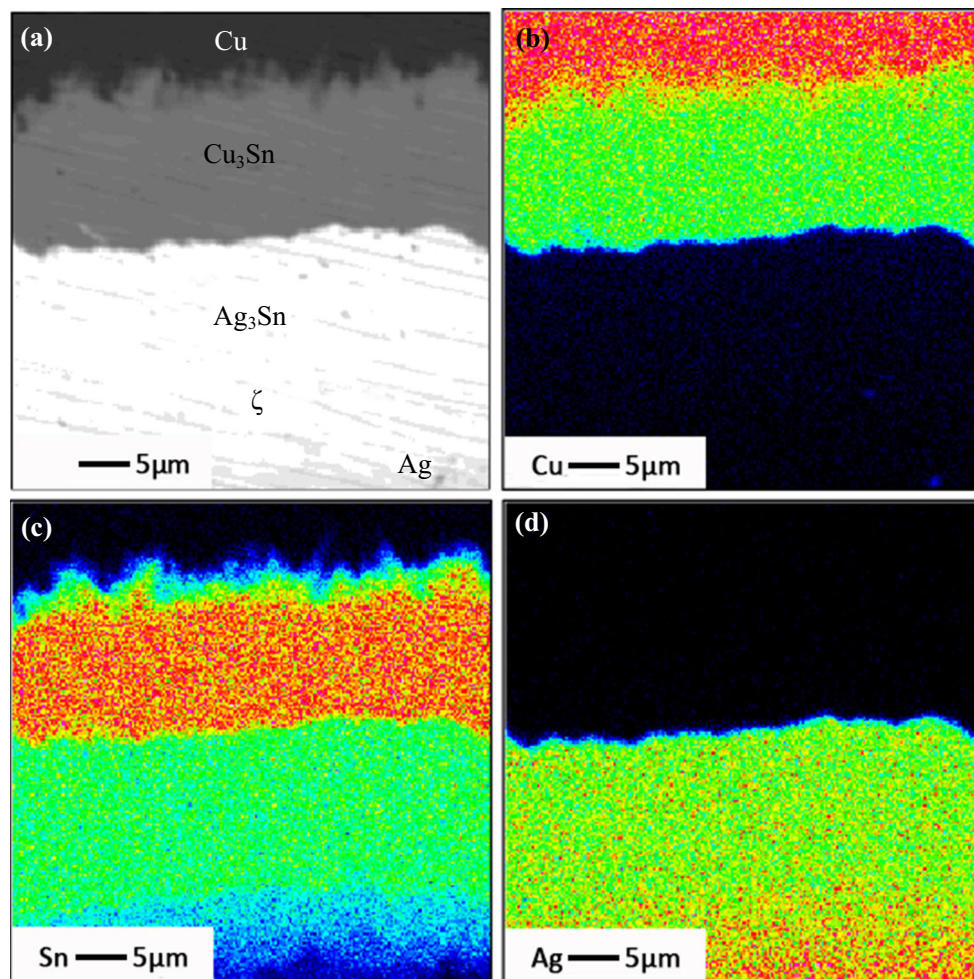


Fig. 3 EPMA elemental mapping images for Cu, Sn and Ag in the joint bonded at 300 °C for 420 min

transgranular fracture facets were observed on the Cu and Ag side, but most are intercrystalline mode. Marked zones A and B were Cu_6Sn_5 and Ag_3Sn phase identified by the EDS, respectively, and this revealed that cracks majorly propagated along the $\text{Cu}_6\text{Sn}_5/\text{Ag}_3\text{Sn}$ interface during shear test. However, Cu_3Sn IMCs was not observed on the fracture, which indicated that adhesive strength of $\text{Cu}_6\text{Sn}_5/\text{Cu}_3\text{Sn}$ interface was stronger than that of the $\text{Cu}_6\text{Sn}_5/\text{Ag}_3\text{Sn}$ interface, because some pores were formed at the $\text{Cu}_6\text{Sn}_5/\text{Ag}_3\text{Sn}$ interface (Fig. 7b) and negatively affected their combination.

Figure 8 showed the fracture surface of the joint bonded at 300 °C for 300 min, in which the island-like Cu_6Sn_5 IMCs were dispersedly distributed nearby the $\text{Cu}_3\text{Sn}/\text{Ag}_3\text{Sn}$ interface and the microstructure was mainly composed of Cu_3Sn and Ag_3Sn intermetallic phases. It could be seen that some rock candy shaped structures and shear bands exhibited on the rupture surface, which indicated that cleavage fracture was the fracture mode for this joint. As analyzed in Table 1, Cu_6Sn_5 , Cu_3Sn and Ag_3Sn were all detected both on the Cu and Ag side,

thus, cracks majorly extended in the IMCs layers but not along the $\text{Cu}_3\text{Sn}/\text{Ag}_3\text{Sn}$ interface during the rupture process. It was deduced that the adhesive strength of $\text{Cu}_3\text{Sn}/\text{Ag}_3\text{Sn}$ interface slightly improved in contrast to $\text{Cu}_6\text{Sn}_5/\text{Ag}_3\text{Sn}$ interface based on the shear strength changing with bonding time (Fig. 6). Interestingly, pronounced Ag_3Sn shear band, as shown in Fig. 8c, was found all over the fracture surface on the Ag side, indicating the force direction. In comparison to the brittle Cu–Sn IMCs, Ag_3Sn phase has a better ductility according to their rupture features.

After the Cu_6Sn_5 IMCs was fully converted into Cu_3Sn , as shown in Fig. 9, fracture surface of the joint was observed using SEM. Only Cu_3Sn , no Ag_3Sn or ζ phase, was detected throughout the fracture surface, according to the EDS results. Thus, failure path of this joint propagated in the Cu_3Sn layer. And broken Cu_3Sn presented a rock candy shaped morphology, which revealed cleavage fracture characterization.

Fracture model of different joints was developed based on the above analysis, as shown in Fig. 10. After full

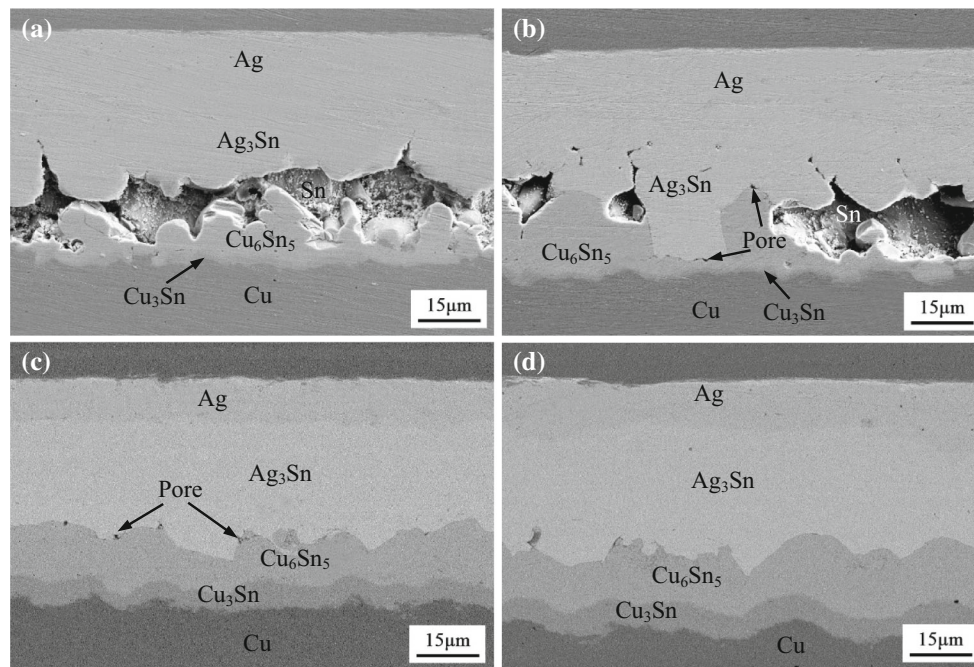
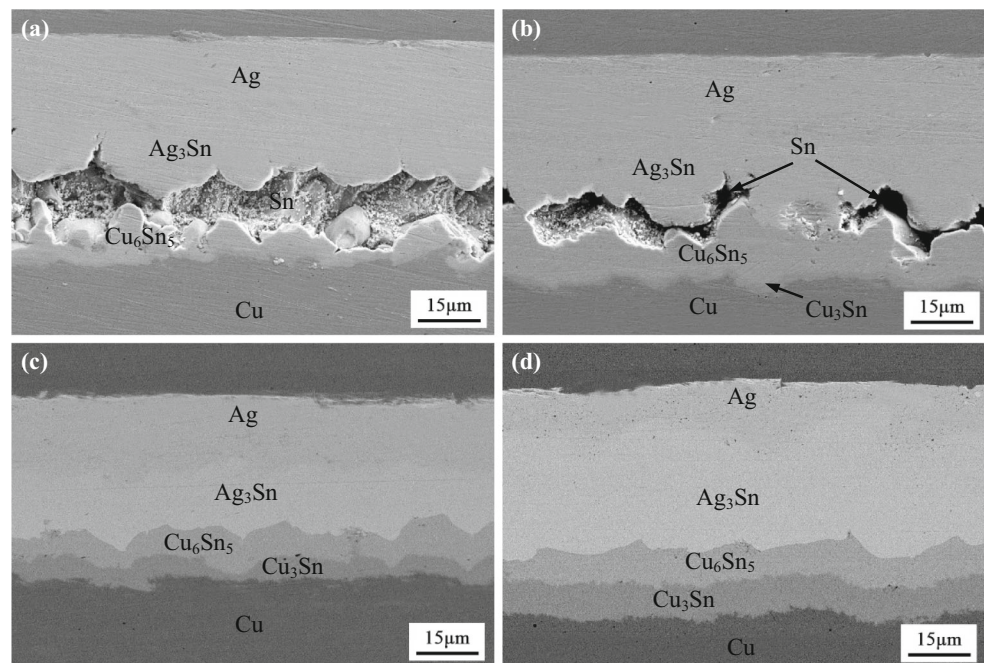


Fig. 4 Cross-sectional microstructure of the joints bonded at 260 °C for **a** 60 min and **b** 150 min in secondary electron mode (residual Sn was removed with etching solution); **c** 300 min and **d** 420 min in backscattered electron mode

Fig. 5 Cross-sectional microstructure of the joints bonded at 340 °C for **a** 15 min and **b** 30 min in secondary-electron mode (residual Sn was removed with etching solution); **c** 60 min and **d** 150 min in backscattered electron mode



consumption of the residual Sn (Fig. 10a), scalloped Ag_3Sn and Cu_6Sn_5 combined with each other but pores remained at the interface, therefore, cracks would initiate at these areas and not only extended along $\text{Cu}_6\text{Sn}_5/\text{Ag}_3\text{Sn}$ interface, but also propagated in the Cu_6Sn_5 and Ag_3Sn crystals for their mutually embedded scallops. As Ag_3Sn combined with Cu_6Sn_5 badly at this time, intergranular fracture

played a key role during shear test. When Cu_6Sn_5 existed as island-like form at the $\text{Cu}_3\text{Sn}/\text{Ag}_3\text{Sn}$ interface (Fig. 10b), failure path dominantly passed through the Cu_3Sn and Ag_3Sn layer, and cut through inlaid Cu_6Sn_5 islands as well. As Cu_6Sn_5 totally converted into Cu_3Sn (Fig. 10c), two interfaces of ζ phase/ Ag_3Sn and $\text{Ag}_3\text{Sn}/\text{Cu}_3\text{Sn}$ remained in the IMCs and combined very well, so

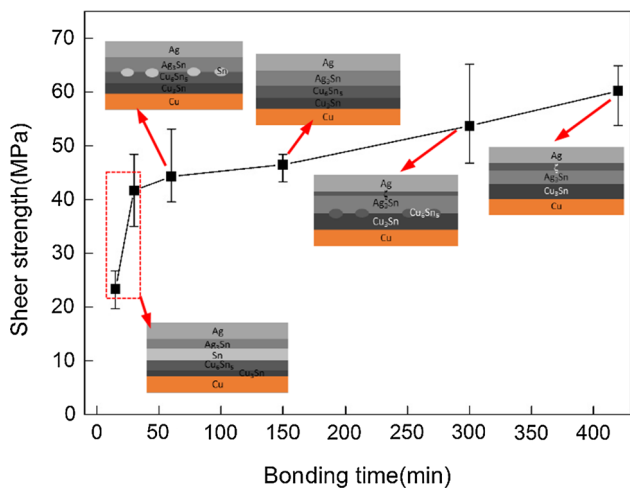


Fig. 6 Dependence of the shear strength of the joints on the bonding time

that cracks propagated throughout Cu_3Sn layer during failure process.

3.3 Mechanism of the combination between Cu–Sn IMCs and Ag–Sn IMCs

As mentioned above, several pores were found that distributed around the $\text{Cu}_6\text{Sn}_5/\text{Ag}_3\text{Sn}$ interface when Cu_6Sn_5 layer initially contacted with the Ag_3Sn layer. Their top-view morphologies were observed by the fracture surface of the corresponding joint, as shown in Fig. 11, and it could be found that pores were situated between either Cu_6Sn_5 scallops or Ag_3Sn scallops due to grain boundary grooving. Bosco proposed that pores in Cu–Sn–Cu TLP-bonded joints formed before the Sn melted, which was caused by Cu/Sn solid-state reaction in heating stage, and Sn coating thickness and heating rate were regarded as the crucial factors [11]. However, this model was not suitable for our bonding configuration, since formation of the IMCs during heating process impossibly occurred in Sn foil bonding

with a low pressure. We considered that such pores were left behind by insufficient filling of the Sn islands entrapped in $\text{Cu}_6\text{Sn}_5/\text{Ag}_3\text{Sn}$ interface which would isothermally convert into IMCs but accompanied by volume shrinkage. As this type of defect was distributed in the space of several IMCs grains, we called it grain boundary pore.

As the top of Cu_6Sn_5 scallops approximately contacted with the opposite Ag_3Sn scallops, growth model in geometry was established to discuss combination mechanism of Ag–Sn and Cu–Sn IMCs. As shown in Fig. 12, two different circumstances, including top-to-top and top-to-root, were distinguished by the coming contact forms of the Cu_6Sn_5 with Ag_3Sn scallops. In detail, the form of top-to-top was the top of Cu_6Sn_5 scallops contacted with the top of Ag_3Sn scallops, while top-to-root was the top/root of Cu_6Sn_5 scallops contacted with the root/top of Ag_3Sn scallops. For the case of top-to-top, molten Sn was isolated into separate areas once the top of Cu_6Sn_5 scallop contacted with the top of Ag_3Sn scallop (Fig. 12a), and they hindered vertical growth of each other so that grew toward the liquid Sn islands. As continued reaction, residual Sn islands was totally consumed and filled with IMCs, and many pores were remained at the grain boundaries (Fig. 12b), besides, no coalescence took place between two opposite IMCs scallops for incapable of elements interdiffusion through the boundary. Then, $\text{Cu}_6\text{Sn}_5/\text{Ag}_3\text{Sn}$ interface formed in the top-to-top form turned into relatively planar, and these areas would rupture along the interface and generate intergranular fracture during the shear test. In fact, Fig. 11 also described the top-view morphology of $\text{Cu}_6\text{Sn}_5/\text{Ag}_3\text{Sn}$ interface for this case somehow. For the case of top-to-root, as depicted in Fig. 12c, d, only if molten Sn was almost consumed, Cu_6Sn_5 and Ag_3Sn layers could contact with each other in theory, and small pores were remained at the top/root of either Cu_6Sn_5 or Ag_3Sn scallops, which was in a good agreement with the experimental observation (Fig. 4c). In addition, either Cu_6Sn_5 or Ag_3Sn layer seemingly embedded into the opposite IMCs and their contacted interface kept

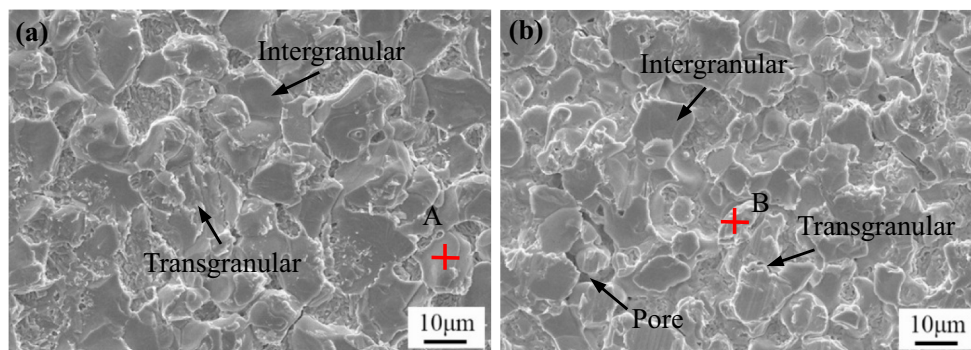


Fig. 7 Fracture surface of the joint bonded at 300 °C for 150 min on the **a** Cu side and **b** Ag side

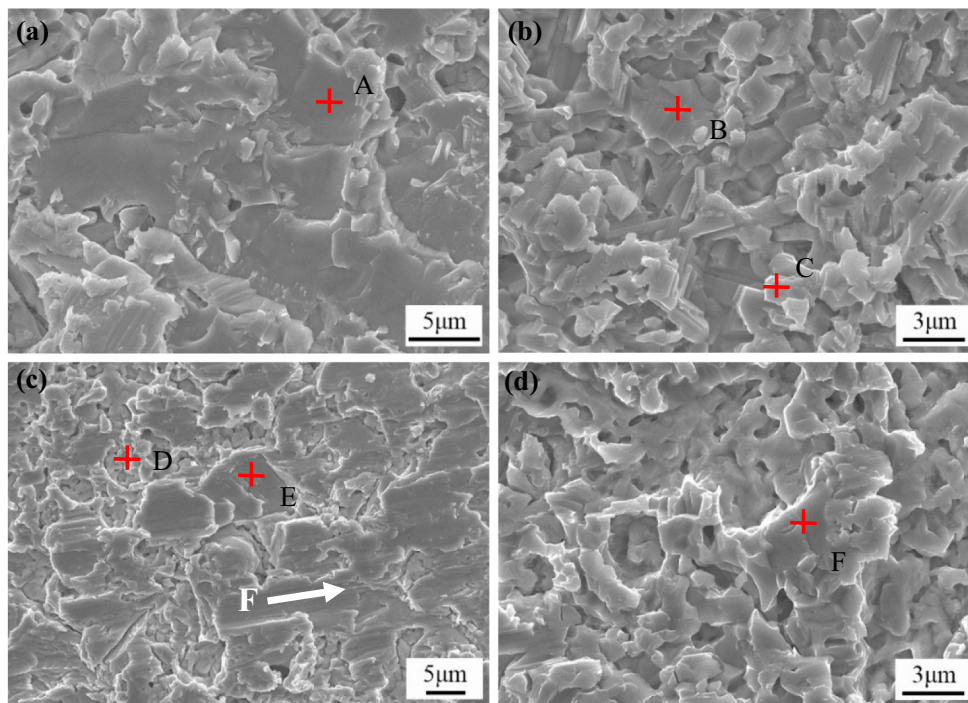
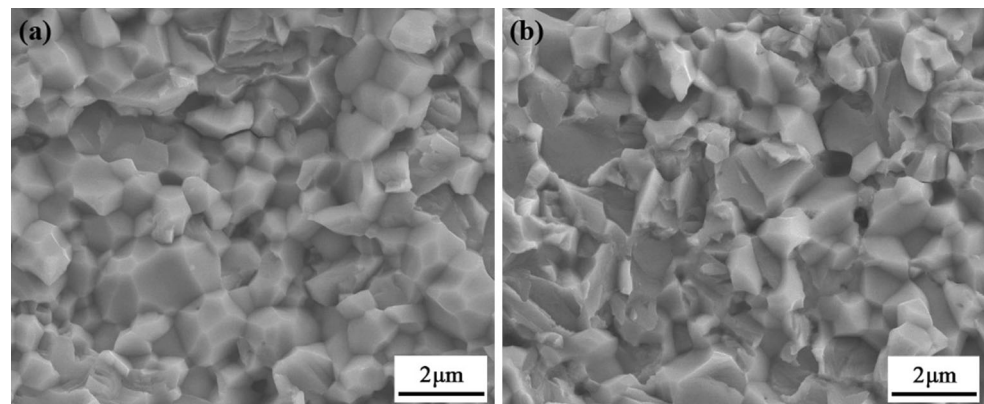


Fig. 8 Fracture surface of the joint bonded at 300 °C for 300 min on the **a, b** Cu side and **c, d** Ag side

Table 1 EDS analysis results of the marked zones in Fig. 8

Marked zone		A	B	C	D	E	F
Composition (at.%)	Cu	55.13	38.09	74.44	68.43	–	63.25
	Sn	44.87	22.02	25.56	26.97	24.19	26.85
	Ag	–	39.89	–	4.60	75.81	9.91
Phase identification		Cu_6Sn_5	$\text{Ag}_3\text{Sn} + \text{Cu}_3\text{Sn}$	Cu_3Sn	$\text{Cu}_3\text{Sn} + \text{Ag}_3\text{Sn}$	Ag_3Sn	$\text{Cu}_3\text{Sn} + \text{Ag}_3\text{Sn}$

Fig. 9 Fracture surface of the joint bonded at 300 °C for 420 min on the **a** Cu side and **b** Ag side



original wave-shaped morphology. This case of areas would be ruptured through the IMCs layer and formed transgranular fracture.

After Cu_6Sn_5 and Ag_3Sn layer were fully contacted with each other, no matter top-to-top or top-to-root combination, the IMCs would continue to transform into more

stable phases, namely, Cu_3Sn and ζ ; and pores distributed around the interface were gradually healed. According to above experimental observation, Cu_3Sn layer grew more rapidly than ζ phase layer under the same condition, and the $\text{Cu}_6\text{Sn}_5/\text{Ag}_3\text{Sn}$ interface evolved into $\text{Cu}_3\text{Sn}/\text{Ag}_3\text{Sn}$ interface firstly, accompanied by vanish of pores. This

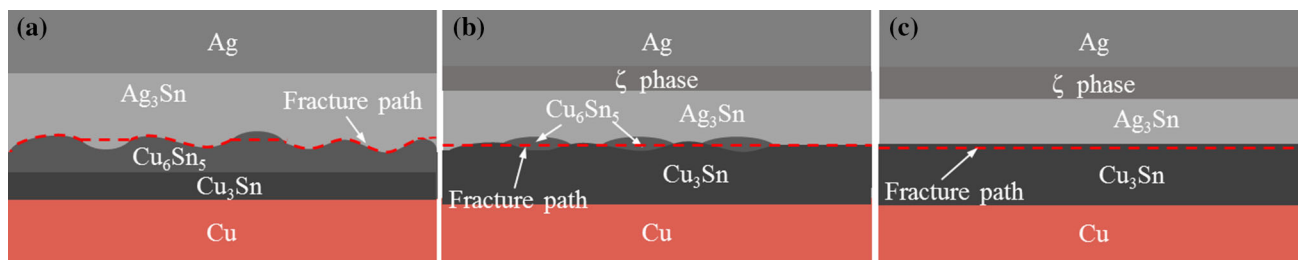


Fig. 10 Fracture model of the joints with different microstructure

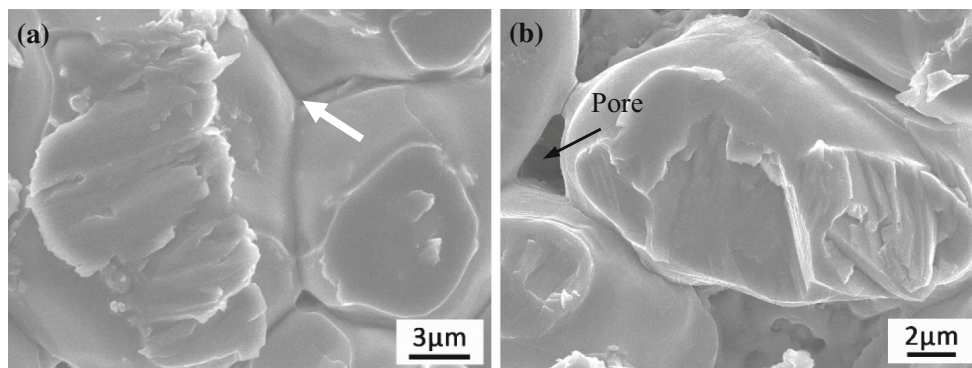
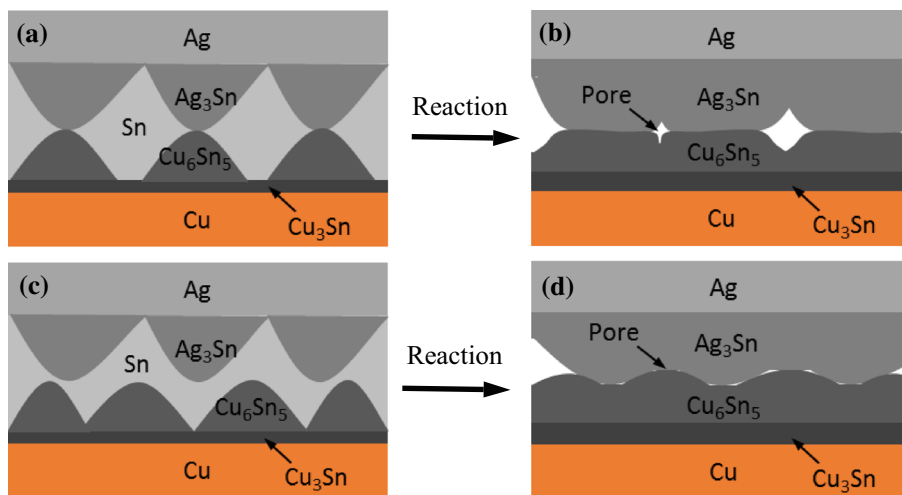


Fig. 11 Grain boundary pores between **a** Cu_6Sn_5 grains or **b** Ag_3Sn grains for the joint bonded at 300 °C for 150 min

Fig. 12 Growth model of the IMCs during Cu_6Sn_5 combination to Ag_3Sn



revealed that self-diffusion probably took place in the reaction process and led to the phenomenon that positions of pores were filled by the IMCs, as a result, the adhesive strength of $\text{Cu}_3\text{Sn}/\text{Ag}_3\text{Sn}$ interface was stronger than that of $\text{Cu}_6\text{Sn}_5/\text{Ag}_3\text{Sn}$ interface.

4 Conclusions

$\text{Cu}/\text{Sn}/\text{Ag}$ system can be perfectly bonded by low temperature transient liquid phase bonding, and the joint has excellent thermal reliability and mechanical property,

which is proven to be a good candidate in application to high temperature electronic packaging. In this work, interfacial reaction and mechanical behaviors for $\text{Cu}/\text{Sn}/\text{Ag}$ system LTTLP bonding at temperatures in a range of 260–340 °C for different time were systematically investigated.

Before full consumption of the molten Sn, Cu and Ag substrate independently reacted with liquid phase, and scalloped Cu_6Sn_5 and Ag_3Sn were formed on the substrate and thickened with increasing bonding temperature and bonding time. After Cu_6Sn_5 contacted with Ag_3Sn , the growth of IMCs on one side was hindered by the opposite

IMCs, which was attributed to incapability of Cu and Ag atoms diffusion through the boundary. A few pores were formed and distributed at the $\text{Cu}_6\text{Sn}_5/\text{Ag}_3\text{Sn}$ interface or between grain boundaries after the residual Sn was totally consumed. With continuing reaction, Cu_6Sn_5 phase transformed into Cu_3Sn phase and a layer of ζ phase was formed at the expense of Ag_3Sn , accompanied by disappearance of the pores. In addition, there were no ternary alloy phases detected for the LTTLP joints.

Shear strength of the joints bonded at 300 °C increased with prolonging bonding time, from 23.4 MPa for 15 min to 60.2 MPa for 420 min, and the adhesive strength of $\text{Cu}_6\text{Sn}_5/\text{Ag}_3\text{Sn}$ interface was weaker than that of the $\text{Cu}_3\text{Sn}/\text{Ag}_3\text{Sn}$ interface due to the formation of pores around the $\text{Cu}_6\text{Sn}_5/\text{Ag}_3\text{Sn}$ interface. At the beginning of the combination of Cu_6Sn_5 and Ag_3Sn layer, cracks initiated in the pore and mainly propagated along the $\text{Cu}_6\text{Sn}_5/\text{Ag}_3\text{Sn}$ interface during shear test. When Cu_6Sn_5 particles were dispersedly distributed at the $\text{Cu}_3\text{Sn}/\text{Ag}_3\text{Sn}$ interface, fracture path dominantly passed through Cu_3Sn and Ag_3Sn layer, and cut open Cu_6Sn_5 particles as well. For the joint composed of a lamellar structure of $\text{Cu}_3\text{Sn}/\text{Ag}_3\text{Sn}/\zeta$ phase, cracks merely extended in the Cu_3Sn layer.

Acknowledgments This research is financially supported by the National Science Foundation of China under Grant No. 51375260, which entitled “Technology and Mechanism of Low Temperature Transient Liquid Phase Bonding”.

Open Access This article is distributed under the terms of the Creative Commons Attribution 4.0 International License (<http://creativecommons.org/licenses/by/4.0/>), which permits unrestricted use, distribution, and reproduction in any medium, provided you give appropriate credit to the original author(s) and the source, provide a link to the Creative Commons license, and indicate if changes were made.

References

1. R.W. Johnson, C. Wang, Y. Liu, J.D. Scofield, IEEE Trans. Electron. Packag. Manuf. **30**, 182 (2007)

2. R.W. Johnson, J.L. Evans, P. Jacobsen, J.R.R. Thompson, M. Christopher, IEEE Trans. Electron. Packag. Manuf. **27**, 164 (2004)
3. P.G. Neudeck, R.S. Okojie, L. Chen, Proc. IEEE **90**, 1065 (2002)
4. V.R. Manikam, K.Y. Cheong, IEEE Trans. Compon. Packag. Manuf. Technol. **1**, 457 (2011)
5. E. Jang, S. Hyun, H. Lee, Y. Park, J. Electron. Mater. **38**, 2449 (2009)
6. S. Menon, E. George, M. Osterman, M. Pecht, J. Mater. Sci. Mater. Electron. **26**, 4021 (2015)
7. K.S. Siow, J. Alloys Compd. **514**, 6 (2012)
8. H. Liu, K. Wang, K.E. Aasmundtveit, N. Hoivik, J. Electron. Mater. **41**, 2453 (2012)
9. S. Sommadossi, W. Gust, E.J. Mittemeijer, Mater. Chem. Phys. **77**, 924 (2003)
10. L. Bernstein, J. Electrochem. Soc. **113**, 1282 (1966)
11. N.S. Bosco, F.W. Zok, Acta Mater. **52**, 2965 (2004)
12. J.F. Li, P.A. Agyakwa, C.M. Johnson, Acta Mater. **58**, 3429 (2010)
13. J.F. Li, P.A. Agyakwa, C.M. Johnson, Acta Mater. **59**, 1198 (2011)
14. T.A. Tollefsen, A. Larsson, O.M.L. Vvik, K. Aasmundtveit, Metall. Mater. Trans. B **43**, 397 (2012)
15. W.P. Lin, C.C. Lee, IEEE Trans. Compon. Packag. Manuf. Technol. **1**, 1311 (2011)
16. F.S. Shieu, Z.C. Chang, J.G. Sheen, C.F. Chen, Intermetallics **8**, 623 (2000)
17. C. Hang, Y. Tian, R. Zhang, D. Yang, J. Mater. Sci. Mater. Electron. **24**, 3905 (2013)
18. Y. Chien, Y. Huang, R. Tzeng, M. Shy, T. Lin, K. Chen, C. Chiu, C. Chuang, W. Hwang, J. Chiou, H. Tong, K. Chen, IEEE Trans. Electron Devices **61**, 1131 (2014)
19. T.A. Tollefsen, A. Larsson, M.M.V. Taklo, A. Neels, X. Maeder, K.H. Ydalsvik, D.W. Breiby, K. Aasmundtveit, Metall. Mater. Trans. B **44**, 406 (2013)
20. D. Gur, M. Bamberger, Acta Mater. **46**, 4917 (1998)
21. T. Studnitzky, R. Schmid-Fetzer, J. Electron. Mater. **32**, 70 (2003)
22. O.H. Baker, *ASM Handbook: Alloy Phase Diagrams Version 3* (ASM International, Metals Park, OH, 1992)
23. Y. Tian, C. Hang, X. Zhao, B. Liu, N. Wang, C. Wang, J. Mater. Sci. Mater. Electron. **25**, 4170 (2014)
24. R.I. Rodriguez, D. Ibitayo, P.O. Quintero, IEEE Trans. Compon. Packag. Manuf. Technol. **3**, 549 (2013)
25. W.Y. Sang, M.D. Glover, H.A. Mantooth, K. Shiozaki, J. Micromech. Microeng. **23**, 15017 (2012)